Hydrothermal Synthesis, Structural Investigation, Photoluminescence Features, and Emission Quantum Yield of Eu and Eu−Gd Silicates with Apatite-Type Structure

Stanislav Ferdov,[†,‡,§] Rute A. Sá Ferreira,[‡] and Zhi Lin*[,†]

Departments of Chemistry and Physics, CICECO, University of Aveiro, 3810-193 Aveiro, Portugal

Received July 25, 2006. Revised Manuscript Received October 2, 2006

For the first time, $Eu_{8.18}Na_{1.08}(SiO_4)_6(OH)_{1.62-2y}O_y$ (Eu apatite) and $Eu_{3.96}Gd_{3.96}Na_{1.2}(SiO_4)_6(OH)_{1.86-2y}O_y$ (Eu−Gd apatite) were synthesized at mild hydrothermal conditions. Powder X-ray analysis suggested a preferential substitution of Ln^{3+} by Na^+ ions in 4f position for both materials. The substitution of Eu^{3+} by Gd^{3+} ions alters the distribution of the Ln^{3+} ions between 4f and 6h sites, which impacts their local symmetry, optical properties, and quantum efficiency. These materials are efficient room-temperature emitters with a maximum external quantum yield of ca. 21.4%. The abnormal increase in the relative intensity of the Eu^{3+} intra-$4f^6$ $^5D_0 \rightarrow {}^7F_4$ transition is attributed to the presence of interstitial oxygen or incommensurate ordering of the oxygen around the 6h position, which results in a distortion of the Eu^{3+} local symmetry. Evidence of concentration quenching effects will be discussed based on the $^5D_0$ lifetime and the emission quantum yield dependence on the Eu^{3+} concentration.

1. Introduction

Compounds with the apatite-type structure have been widely studied due to their potential applications as biomaterials,[1] catalysts,[2] ionic exchangers,[3] oxide ion conductors, and luminescent materials.[4] Among the family of apatite materials, lanthanide (Ln^{3+}) silicate compounds (Ln apatite) are attracting considerable interest as a new class of oxygen anion conductors as they show higher oxygen ion conductivity (below 600 °C) than that of the stabilized zirconia.[5] To date, silicon-based lanthanide apatites have been prepared as polycrystalline samples and single crystals. The single crystals have been prepared by the floating zone method,[6] while the polycrystalline samples were synthesized through solid-state reactions[7] and sol−gel method,[8] generally at temperatures over 1000 °C. Concerning the silicon-based lanthanide hydroxyapatites, there are reports for the synthesis via solid-state reactions, and high temperature (500−700 °C) and pressure (2 kbar) hydrothermal process.[9,10] However, there is no report for the successful synthesis of silicate oxy-hydroxyapatites.

Except for the use as oxygen ion conductors Ln apatites have been extensively studied due to their great interest as fluorescent lamp phosphors[11,12] and as potential laser host materials.[13] When activated by trivalent lanthanide ions, these apatites have been found to exhibit favorable laser spectroscopic properties due to their unusually high crystal field splitting.[14]

Depending on the O^{2-}/OH^- ratio in the apatite structure, this material could be described as oxyapatite, hydroxyapatite, or oxy-hydroxyapatite. There are only a few reports investigating lanthanide (in particular, Eu^{3+}) doped silicate oxyapatites[9,15−17] and no report has been published on photoluminescence properties of hyrdoxy- and oxy-hydroxyapatite silicates. In this work we report for the first time a mild hydrothermal synthesis, photoluminescence properties, and emission quantum yield of Eu^{3+} and Eu^{3+}−Gd^{3+} oxy-hydroxyapatite silicates.

2. Experimental Section

2.1. Syntheses. The hydrothermal synthesis of Eu apatite was carried out from gels with the following chemical composition: 5−14:1−2:1−2:300−700 Na_2O:Eu_2O_3:SiO_2:H_2O. In a typical synthesis, 0.16 g of SiO_2 (Aldrich) was added to a solution of 0.76 g of NaOH (Aldrich) in 3.72 g of distilled water. Subsequently, 1 g of $EuCl_3 \cdot 6H_2O$ (Aldrich) in 3.68 g of distilled water was added to the previous solution. The resulting gel was homogenized for

* To whom correspondence should be addressed. E-mail: zlin@ciceco.ua.pt. Tel.: 351 234401519. Fax: 351 234370084.
† Department of Chemistry.
‡ Department of Physics.
§ On leave from the Central Laboratory of Mineralogy and Crystallography, Bulgarian Academy of Sciences.

(1) Suchanek, W.; Yoshimura, M. *J. Mater. Res.* **1998**, *13*, 94.
(2) Monma, H. *J. Catal.* **1982**, *75*, 200.
(3) Suzuki, T. *Gypsum Lime* **1986**, *204*, 316.
(4) Blasse, G. *Mater. Chem. Phys.* **1987**, *16*, 201.
(5) Higuchi, Y.; Sugawara, M.; Hawazaki, K.; Uewatsu, K.; Nakayama, S. U.S. Patent 2004/0161651 A1.
(6) Higuchi, M.; Katase, H.; Kodaria, K.; Nakayama, S. *J. Mater. Sci. Lett.* **2000**, *19*, 91.
(7) Nakayama, S.; Sakamoto, M. *J. Eur. Ceram. Soc.* **1998**, *18*, 1413.
(8) Tao, S.; Irvine, J. T. S. *Mater. Res. Bull.* **2001**, *36*, 1245.
(9) Ito, J. *Am. Mineral.* **1968**, *53*, 890.
(10) Wang, C.; Lin, X.; Fleet, M. E.; Feng S.; Xu, R. *J. Solid State Chem.* In press.
(11) Butler, K. H. *Fluorescent Lamp Phosphors*; Pennsylvania State University Press: University Park, PA, 1986.
(12) Davis, T. S.; Kreidler, E. R.; Parodi J. A.; Soules, T. F. *J. Lumin.* **1971**, *4*, 48
(13) Budin, J. C.; Michel; J. C.; Auzel, F. *J. Appl. Phys.* **1979**, *50*, 641.
(14) Spariosu, K.; Stultz;, R. D.; Brinbaum, B.; Allik, T. H.; Hutchinson, J. A. *Appl. Phys. Lett.* **1993**, *63*, 2763.
(15) Blasse, G. *J. Solid State Chem.* **1975**, *14*, 181.
(16) Blasse, G.; Bril, A. *J. Inorg. Nucl. Chem.* **1967**, *29*, 2231.
(17) Isaacs, T. J. *J. Electrochem. Soc.* **1973**, *120*, 654.

10.1021/cm0617384 CCC: $33.50
Published on Web 11/17/2006

40 min and then transferred into a Teflon-lined autoclave. The crystallization was performed under static conditions at 230 °C for 6 days. After fast cooling with flowing water the run product was filtered with distilled water and dried at 50 °C for 1 day. The same procedure was applied for the preparation of Eu-Gd apatite using gels with the following chemical composition: 5−14:0.5−2:0.5−2:2:300−700 Na_2O:Eu_2O_3:Gd_2O_3:SiO_2:H_2O, where the run product resulted in the Eu−Gd silicate with the apatite structure. $GdCl_3 \cdot 6H_2O$ (Aldrich) was used as a source of Gd^{3+}.

2.2. Characterization. Chemical analysis (EDS) was carried out using a Römteck EDS System attached to a scanning electron microscope Hitachi S-4100. Powder X-ray diffraction (XRD) data were collected on a Philips X'Pert MPD diffractometer (Cu Kα X-radiation) with a curved graphite monochromator, a fixed divergence slit of 0.25°, and a flat plate sample holder, in a Bragg−Brentano para-focusing optics configuration. The diffraction intensity was collected by the step scan method (step 0.02° and time 30 s) in the 2θ range between 9 and 140°. Fourier transform infrared spectra (FTIR) of powdered samples suspended in KBr pallets were acquired between 400 and 4000 cm^{-1} using a Mattson Mod 7000 spectrometer. The luminescence spectra were recorded between 14 K and room temperature with a modular double-grating excitation spectrofluorimeter with a TRIAX 320 emission monochromator (Fluorolog-3, Jobin Yvon-Spex) coupled to a R928 Hamamatsu photomultiplier, using the front face acquisition mode. The excitation source was a 450 W Xe arc lamp. The emission spectra were corrected for detection and optical spectral response of the spectrofluorimeter and the excitation spectra were corrected for the spectral distribution of the lamp intensity using a photodiode reference detector. The lifetime measurements were acquired with the setup described for the luminescence spectra using a pulsed Xe−Hg lamp (6 μs pulse at half-width and 20−30 μs tail). The absolute emission quantum yields (ϕ) were measured at room temperature using the technique for powdered samples described by Wrighton et al.[18] through $\phi = A/(R_s - R_{apatite})$, where A is the area under the silicates' emission spectra and R_s and $R_{apatite}$ are the diffuse reflectance—with respect to a fixed wavelength—of the reflecting standard and of the silicates, respectively. Diffuse reflectance and emission spectra were acquired with the experimental setup used to detect photoluminescence. To have absolute intensity values, $BaSO_4$ was used as a reflecting standard ($r = 91\%$). The same experimental conditions, namely, position of the hybrids/standard holder, excitation and detection monochromator slits (0.2 mm), and optical alignment, were fixed. To prevent insufficient absorption of the exciting radiation, a powder layer around 2 mm was used and utmost care was taken to ensure that only the sample was illuminated, to diminish the quantity of light scattered by the front sample holder. Four measurements were carried out so that the presented values correspond to the arithmetic mean values. The errors in the quantum yield values associated with this technique were estimated within 25%.[19]

3. Results and Discussion

3.1. Infrared (FTIR) Spectroscopy. The FTIR spectra of both samples are very similar (Figure 1). The spectrum of the Eu apatite exhibits bands at 3439, 1634, 1392, 983, 559, and 501 cm^{-1} while the bands of the Eu−Gd apatite are centered at 3439, 1634, 1392, 981, 561, and 503 cm^{-1}. The broadband between 3300 and 3660 cm^{-1} arises from the O−H bond stretching modes and demonstrates a presence of hydrous species. The bands at 3439 and 1634 cm^{-1} (H−O−H bond bending) show the presence of surface water molecules, whereas the shoulder at 3570 cm^{-1} indicates the existence of M−OH groups.[20] Generally, in the hydroxyapatites the band corresponding to the O−H stretching mode appears as a narrow peak;[21] however, in the spectra of Figure 1 it appears as a shoulder. Moreover, the OH librational mode usually detected in hydroxyapatites was not observed, suggesting a low content of OH^- ions. The presence of mixed valence cations in the apatite structure could result in not only the creation of vacancies but also the coexistence of OH^- and O^{2-} ions, leading to the formation of oxyhydroxyapatites.[22] The weak band at 1392 cm^{-1} results from a small amount of carbonate species adsorbed from ambient on the particle surface. The bands at 981 and 983 cm^{-1} are attributed to Si−O stretching modes[23] and the ones at 561, 503 cm^{-1} and 559, 501 cm^{-1}, for the Eu apatite and the Eu−Gd apatite, respectively, are assigned to Ln−O vibration modes.[24]

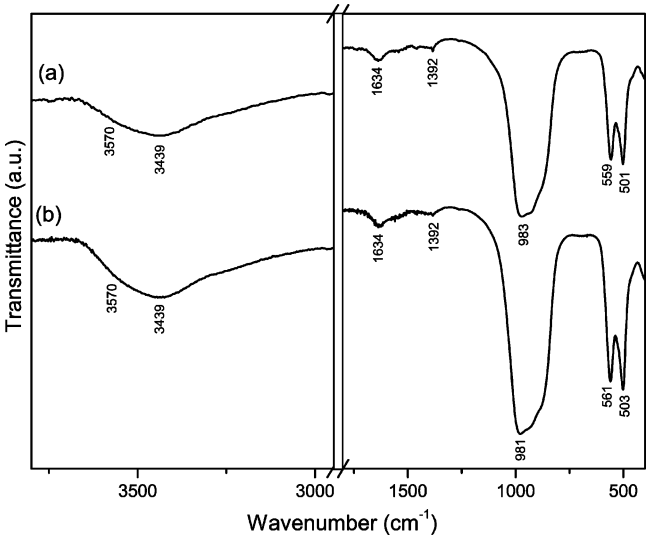

Figure 1. FTIR spectra of (a) Eu apatite and (b) Eu−Gd apatite.

3.2. Rietveld Refinement. The as-synthesized lanthanide silicates crystallize with regular apatite-type structure (Figure 2). Within the experimental error, the chemical analysis by EDS supports Eu:Na:Si (1:0.12:0.72) and Eu:Gd:Na:Si (0.4:0.5:0.15:0.76) ratios obtained by powder XRD.

The structures of $Eu_{8.18}Na_{1.08}(SiO_4)_6(OH)_{1.62-2y}O_y$ and $Eu_{3.96}Gd_{3.96}Na_{1.2}(SiO_4)_6(OH)_{1.86-2y}O_y$ were refined by the program FULLPROF[25] starting from a model of Ho hydroxyapatite with the space group $P6_3/m$ ($n = 176$).[26] Le

(18) Wrighton, M. S.; Gingley, D. S.; Morse, D. L. *J. Phys. Chem.* **1974**, *78*, 2229.
(19) Bril, A.; De, Jager-Veenis, A. W. *J. Res. Nat. Bureau Stand.* **1976**, *80A*, 401.
(20) Beran, A.; Voll, D.; Schneider, H. In *Spectroscopic Methods in Mineralogy*; Beran, A., Libowitzky, E., Eds.; Eötvös University Press: Budapest, 2004.
(21) Fowler, B. O. *Inorg. Chem.* **1974**, *13*, 194.
(22) Serret, A; Cabañas, M. V.; Vallet-Regi, M. *Chem. Mater.* **2000**, *12*, 3836.
(23) Mihailova, B.; Valtchev, V.; Mintova, S.; Konstantinov, L. *Zeolites* **1996**, *16*, 22.
(24) Kannan, R.; Mohan, S. *Mater. Sci. Eng.* **2001**, *B86*, 113.
(25) Rodriguez-Carvajal, J. FULLPROF, Program for Rietveld Refinement and Pattern Matching Analysis. In *Abstracts of the Satellite Meeting on Powder Diffraction of the XVth Congress of the International Union of Crystallography*, Toulouse, France, July 1990; p 127.
(26) Fleet, M. E.; Xiaoyang, L. *J. Solid State Chem.* **2005**, *178*, 3275.

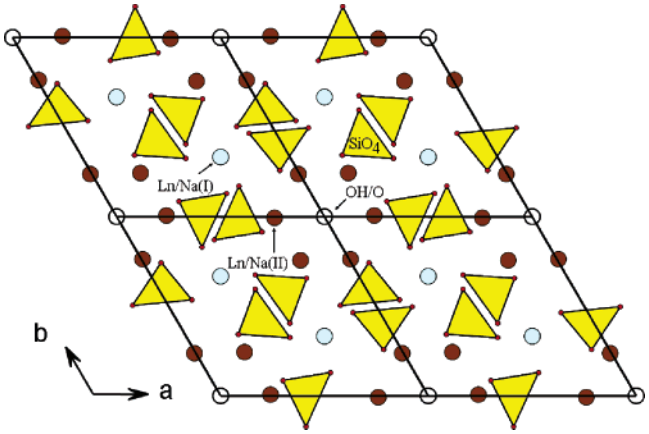

Figure 2. View of the refined crystal structure of the oxy-hydroxyapatites along [001].

Bail Fitting was first performed to get suitable parameters for the peak function, and in the meantime the lattice parameters and zero point were refined.

As the detected sodium ions could reside in both 4f (I) and 6h (II) positions, the occupancy factors of Ln^{3+} and Na^{+} on both sites were allowed to vary (taking into account the chemical composition as well as their similar chemical character, Eu^{3+} and Gd^{3+} ions are considered as randomly distributed between 6h and 4f sites with a total ratio close to 1:1 − Eu−Gd phase). The occupancy of Si was optimized with a restraint of a full occupation of the site. Then, the refinement of the occupancy of Na^{+} and Ln^{3+} ions on both cation sites were restrained to take into account the chemical analysis ratios.

When monovalent cation (Na^{+}) substitutes a trivalent one (Eu^{3+}, Gd^{3+}), two possibilities can be considered to keep the charge balance: creation of cationic and anionic vacancies or increasing of the number of OH^{-} ions at the expense of O^{2-} ions. Taking into account the powder XRD and FTIR data, it could be a combination of both effects, showing the presence of two kinds of charge carriers; i.e., OH^{-} and O^{2-} determine the phases as oxy-hydroxyapatite ones.

To fulfill the condition of charge neutrality, the number of OH^{-} ions are assumed to be 1.62 (Eu apatite) and 1.86 (Eu−Gd apatite). However, considering the FTIR data, the refined 4e position might represent an average of OH^{-} and O^{2-} ions and its chemical composition could be as follows: $(OH)_{1.62-2y}O_y\square_{0.38+y}$ (Eu apatite) and $(OH)_{1.86-2y}O_y\square_{0.18+y}$ (Eu−Gd apatite), where □ represents the vacancies.

Because of the presence of cationic vacancies, additional complexity is introduced for 4f and 6h site occupations. Considering that the Rietveld refinement was performed from conventional powder X-ray data, we must note that the refinement is not possibly a unique one for Ln/Na/vacancy distributions. Details from our best Rietveld refinement are reported in Table 1. Refined atomic coordinates and isotropic and displacement parameters are shown in Table 2. Selected interatomic distances of the refinement are gathered in Table 3. The observed, calculated, and difference profiles are given in Figure 3.

The crystal structure of both phases is built from an isolated SiO_4 tetrahedron and two different kinds of polyhedra corresponding to 4f (nine-coordinated) and 6h (seven-coordinated) Wyckoff positions that are occupied by Eu^{3+}, Na^{+} or Eu^{3+}, Na^{+}, and Gd^{3+}. Si atoms in the Eu−Gd apatite form quite short Si−O bonds (average 1.569 Å) when compared with the ones of the Eu apatite (average 1.617 Å). In both phases the atoms that reside in the 4f position are connected to nine oxygen atoms with M(Ln^{3+},Na^{+})−O average distance of 2.522 Å (Eu apatite) and 2.560 Å (Eu−Gd apatite). When the M−OH bond is omitted, the average bond distance for the atoms in the 6h position is equal for both apatites, 2.490 Å.

Table 1. Crystal Data on (A) Eu Apatite and (B) Eu−Gd Apatite

	(A)	(B)
space group	$P6_3/m$	$P6_3/m$
cell parameters (Å)		
$a = b$	9.4812(8)	9.4940(1)
c	6.9139(2)	6.8975(3)
volume (Å^3)	538.2(6)	538.4(2)
R_p	13.8	13.8
R_{wp}	16.6	15.1
R_{exp}	14.4	13.9
R_B	3.67	2.69
R_F	3.13	2.26
χ^2	1.33	1.20

The obtained results also imply a preference for the Na^{+} ions to occupy the 4f site in both apatites and more pronounced for the Eu apatite. The distribution of the Eu^{3+} and Gd^{3+} ions between the 6h and 4f positions is indistinguishable because of their close chemical character. However, the detected variations in the unit cell axis of both samples are dependent on the isomorphous substitution of Eu^{3+} ions by Na^{+} or/and Gd^{3+} ions. It is well-known that the unit cell parameters of lanthanide apatites are strongly dependent on the chemical content of the 6h and 4f sites. In lanthanide apatites with the space group $P6_3/m$, substitutions at the 6h lattice site result mostly in variation in the *a* axis while substitutions at the 4f site do not affect significantly the *a* axis since shorter bonds of the 6h position lie in the direction [*hk*0].[27] It is also known that the variation in *c* lattice parameter depends mainly on the substitutions at the 4f site. According to these facts and to the different ionic radii among Eu^{3+} (seven-coordinated, 1.01 Å; nine-coordinated, 1.12 Å), Gd^{3+} (seven-coordinated, 1 Å; nine-coordinated, 1.107 Å), and Na^{+} (seven-coordinated, 1.12 Å; nine-coordinated, 1.24 Å),[28] the unit cell parameters of $Eu_{8.18}Na_{1.08}(SiO_4)_6(OH)_{1.62-2y}O_y$ show expected extension along the *c* axis and shortening along the *a* axis, when compared with those in $Eu_{3.96}Gd_{3.96}Na_{1.2}(SiO_4)_6(OH)_{1.86-2y}O_y$ (Table 1). From the evolution of the unit cell parameters of Eu−Gd apatite, it could also be suggested that the 4f position is more populated with Gd^{3+} ions than with Eu^{3+} ions. Except for variations in the unit cell parameters the isomorphous substitution causes slight displacements of the atom positions which is pronounced in the case of hydroxyl oxygen O(H). The detected shift from $z = 0.187(3)$ (Eu apatite) to $z = 0.171(3)$ (Eu−Gd apatite) results in a longer M−OH bond (Table 3). This suggests that the 6h position in the Eu−Gd apatite is more populated with Na^{+} ions than that of the Eu apatite because the attraction between the Na^{+} and OH^{-} ions is less intense than the one between Ln^{3+} and OH^{-}.

(27) Felsche, J. *J. Solid State Chem.* **1972**, *5*, 266.
(28) Shannon, R. D. *Acta. Crystallogr.* **1976** *A32* 751.

Table 2. Atomic Coordinates and Equivalent Isotropic Displacement Parameters

atom	Wyck	*x*/*a*	*y*/*b*	*z*/*c*	S.O.F.	B_{iso} (Å^2)
			(A) Eu Apatite			
Eu/Na(1)	4f	$^2/_3$	$^1/_3$	0.0013(7)	0.77/0.21	0.627(2)
Eu/Na(2)	6h	0.9930(3)	0.2373(2)	$^1/_4$	0.85/0.04	0.244(8)
Si	6h	0.3725(8)	0.4034(8)	$^1/_4$	1	0.672(9)
O(1)	6h	0.4961(1)	0.3255(1)	$^1/_4$	1	1.102(0)
O(2)	6h	0.4644(1)	0.5943(2)	$^1/_4$	1	1.102(0)
O(3)	12i	0.2580(9)	0.3439(9)	0.0598(1)	1	1.102(0)
O(H)	4e	0	0	0.187(3)	0.405	1.102(0)
			(B) Eu−Gd Apatite			
Ln/Na(1)	4f	$^2/_3$	$^1/_3$	−0.0002(8)	0.75/0.18	0.727(1)
Ln/Na(2)	6h	0.9924(4)	0.2420(3)	$^1/_4$	0.82/0.08	0.494(6)
Si	6h	0.3684(9)	0.3982(8)	$^1/_4$	1	0.158(9)
O(1)	6h	0.4932(2)	0.3333(2)	$^1/_4$	1	1.492(8)
O(2)	6h	0.4654(2)	0.5843(2)	$^1/_4$	1	1.492(8)
O(3)	12i	0.2591(9)	0.3434(1)	0.0614(1)	1	1.492(8)
O(H)	4e	0	0	0.171(3)	0.465	1.492(8)

Table 3. Selected Bond Distances (Å) for (A) Eu Apatite and (B) Eu−Gd Apatite

(A) Eu apatite			(B) Eu-Gd apatite		
Eu|Na1	O1	2.336(1) [×3]	Ln|Na1	O1	2.385(3) [×3]
	O2	2.426(2) [×3]		O2	2.476(4) [×3]
	O3	2.804(9) [×3]		O3	2.816(2) [×3]
Eu|Na2	O1	2.758(5)	Ln|Na2	O1	2.785(5)
	O2	2.452(1)		O2	2.413(1)
	O3	2.309(3) [×2]		O3	2.299(6) [×2]
	O3	2.554(3) [×2]		O3	2.567(6) [×2]
	OH(4)	2.325(0)		OH(4)	2.397(2)
Si	O1	1.668(6)	Si	O1	1.585(4)
	O2	1.567(8)		O2	1.530(6)
	O3	1.616(7) [×2]		O3	1.581(1) [×2]

3.3. Photoluminescence Spectroscopy. The low-temperature excitation spectrum of the Eu apatite monitored within the $^5D_0 \rightarrow {}^7F_2$ lines is depicted in Figure 4. The spectrum consists of a large broadband peaking at ca. 248 nm and of a series of sharp lines ascribed to intra-4f^6 transitions within the Eu^{3+} 4f^6 electronic configuration. The broadband may be related to the $O^{2-} \rightarrow Eu^{3+}$ ligand-to-metal charge transfer (LMCT) bands formed by the overlap between the intra-4f^6 levels and the orbitals from the oxygen atoms, Eu−O−Eu and Eu−O−Si.[16,17] The intensity of the LMCT band is higher than that of the intra-4f^6 lines, indicating that, at 14 K, the efficiency of the energy conversion from the LMCT states to the Eu^{3+} emitting levels is more efficient than direct excitation into the Eu^{3+} intra-4f^6 levels. Increasing the temperature up to 300 K, there is a decrease in the relative intensity of the broad LMCT bands with respect to the intensity of the intra-4f^6 lines, indicating that the energy conversion of the LMCT states to the Eu^{3+} emitting levels may be thermally deactivated, supporting the LMCT nature of the broadband.[29] The excitation spectrum of the Eu−Gd apatite (not shown) resembles those of the Eu apatite, indicting that the Eu^{3+} sensitization processes are essentially the same in both materials.

The larger overlap between the $O^{2-} \rightarrow Eu^{3+}$ LMCT states and the Eu^{3+} excited levels occurs for the $^5I_6$ level. As the LMCT states are placed well above such Eu^{3+} level, energy-transfer processes between them are active within the temperature range 14−300 K. The intramolecular energy-transfer processes involving lanthanide ions occur essentially via the multipolar and exchange mechanisms.[29] The selection rules are $J + J' \geq \Delta J \geq |J - J'|$ ($J = J' = 0$ excluded) for the former mechanism and $\Delta J = 0, \pm 1$ for the latter one, with J and J' being the total angular momenta of the initial and final state between which the intra-4f^6 transition occurs. For the particular case of intramolecular energy transfer involving the $^5I_6$ level ($J = 6$), we may have $\Delta J = 6$ for the transition involving the $^7F_0$ level ($J = 0$) or $\Delta J = 5$, as the $^7F_1$ ($J = 1$) level is also populated at room temperature. In accordance with these *J*-selection rules, the intramolecular energy transfer from the $O^{2-} \rightarrow Eu^{3+}$ LMCT states to the Eu^{3+} levels occurs mainly via the multipolar mechanism.

Figure 5 compares the low-temperature emission spectra of both materials under excitation via the LMCT band and via intra-4f^6 direct excitation. Under LMCT excitation, the spectra display the typical Eu^{3+} intra-4f^6 transitions ascribed to the $^5D_0 \rightarrow {}^7F_{0-4}$ transitions, the $^5D_0 \rightarrow {}^7F_2$ transition being the more intense one. Luminescence from higher excited levels such as the $^5D_1$ is not detected, indicating very efficient nonradiative relaxation to the $^5D_0$ level. With changing of the excitation from the LMCT band to direct excitation into the 4f^6 levels (395 nm, $^5L_6$ or 465 nm, $^5D_2$), the energy, full-width at half-maximum (fwhm), and Stark components remain unaltered. However, a decrease in the relative intensity of the $^5D_0 \rightarrow {}^7F_2$ transition and an increase in the relative intensity of the remaining ones are observed, the $^5D_0 \rightarrow {}^7F_4$ transition being more intense one. Both the Eu apatite and the Eu−Gd apatite have the same behavior, the latter one being more evident. Such an atypical increase in the relative intensity of the $^5D_0 \rightarrow {}^7F_4$ transition was also observed in other silicates with hexagonal structure.[16] The abnormal increase of the relative intensity of the $^5D_0 \rightarrow {}^7F_4$

(29) de Sá, G. F.; Malta, O. L.; de Mello, Donegá, C.; Simas, A. M.; Longo, R. L.; Santa-Cruz, P. A.; da Silva, E. F, Jr. *Coord. Chem. Rev.* **2000**, *196*, 165.

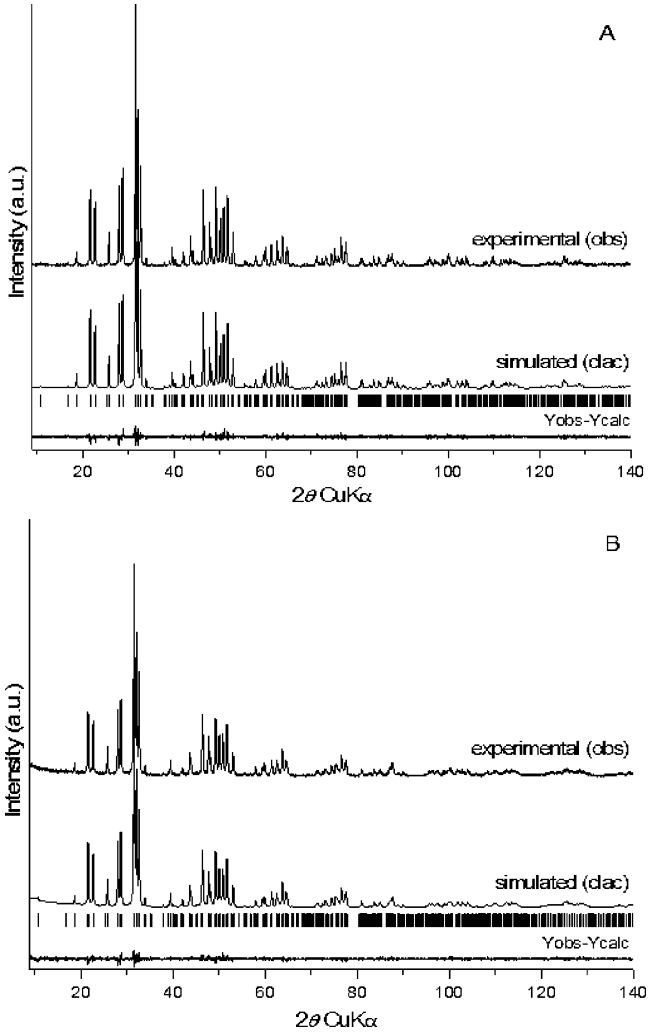

Figure 3. Observed, calculated, and difference powder XRD patterns of (A) Eu apatite and (B) Eu−Gd apatite.

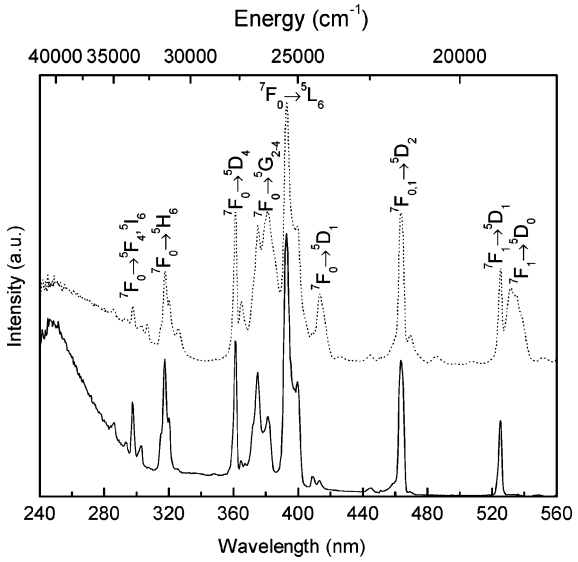

Figure 4. Excitation spectra monitored around 614.5 nm of the Eu apatite obtained at 14 K (solid line) and room temperature (dotted line).

transition was recently related to the distortion of the Eu^{3+} local symmetry group toward a pure inversion center environment.[30] We will return to this point later.

The observed changes in the relative intensity of the Eu^{3+} emission lines as the excitation wavelength is varied are compatible with the presence of two different Eu^{3+}-local coordination sites, as the structural analysis points out. The presence of more than one Eu^{3+} local coordination site is well-established through the analyses of the energy and fwhm of the nondegenerated $^5D_0 \rightarrow {}^7F_0$ transition (E_{0-0} and $fwhm_{0-0}$, respectively). The values for the E_{0-0} and $fwhm_{0-0}$ were obtained by fitting the $^5D_0 \rightarrow {}^7F_0$ transitions in Figure 5 with a single Gaussian function. For all the spectra a good quality fit was obtained ($r^2 > 0.999$), revealing for an excitation wavelength of 248 nm the following values for E_{0-0} and $fwhm_{0-0}$: 17281.1 ± 0.2 cm^{-1} and 44.5 ± 0.5 cm^{-1} (Eu apatite) and 17287.8 ± 0.2 cm^{-1} and 45.8 ± 0.4 cm^{-1} (Eu−Gd apatite), respectively. These values are independent of the selected excitation wavelength. Although only one line is clearly observed for the $^5D_0 \rightarrow {}^7F_0$ transition, the abnormal higher value for the $fwhm_{0-0}$ indicates that the $^5D_0 \rightarrow {}^7F_0$ profiles in Figures 5 may be formed of at least two lines, thus being compatible with the existence of two distinct Eu^{3+} local coordination sites (4f and 6h). Comparing the emission features of the Eu apatite and of the Eu−Gd apatite, the energy and fwhm of the Stark components from the $^5D_0 \rightarrow {}^7F_{0-4}$ transitions are approximately the same, indicating that the Eu^{3+} occupies the same average local environments in both materials. Nevertheless, the E_{0-0} values present a blue-shift (6 cm^{-1}) due to the Eu^{3+} dilution, which may be attributed to the slight difference in the relative intensities of the $^5D_0 \rightarrow {}^7F_0$ lines ascribed to the Eu^{3+} ions in the 4f or the 6h positions, due to the Gd^{3+} replacement of the Eu^{3+} ions in the structure. With increasing of the temperature up to 300 K, the luminescence features resemble those in Figure 5, a smaller relative increase of the $^5D_0 \rightarrow {}^7F_4$ transition with respect to the $^5D_0 \rightarrow {}^7F_2$ one (not shown) being observed.

The apatite lattice has two local sites available for the Eu^{3+} coordination, namely, the 4f position with nine-coordination and the 6h position with seven-coordination numbers. On the basis of crystallographic data, the Eu^{3+} ions occupy the 4f and 6h sites with the local symmetry groups C_3 and Cs, respectively, in a relative occupancy of 40 (4f) and 60% (6h). The number of components for the $D_0 \rightarrow {}^7F_{0-2}$ transitions allowed for the C_3 and Cs symmetry groups is 1, 2, 3 and 1, 3, 5, respectively. The ligand field splitting observed in the emission spectra of the Eu apatite and the Eu−Gd apatite is not consistent with the presence of such two local environments (Figure 5) since it is only possible to clearly discern 3 and 5 Stark components for the $D_0 \rightarrow {}^7F_{1,2}$ transitions. This result is clearly different from those reported for other silicates with hexagonal structures and also with the same two Eu^{3+} crystallographic sites (4f and 6h), where the number of lines observed for the $D_0 \rightarrow {}^7F_{1,2}$ transitions is higher than 3 and 5, respectively.[15−17] Nevertheless, the spectral distribution of the silicates with hexagonal structure was found to be larger than that of silicate materials with orthorhombic or tetragonal symmetries.[16] In the case of the apatite-type materials reported here, the above-mentioned effect could be due to the presence of an interstitial oxygen or incommensurate ordering of the oxygen ions occupying a one-

(30) Sá Ferreira, R. A.; Nobre, S. S.; Granadeiro, C. M.; Nogueira, H. I. S.; Carlos, L. D.; Malta, O. L. *J. Lumin.* **2006**, *121*, 561.

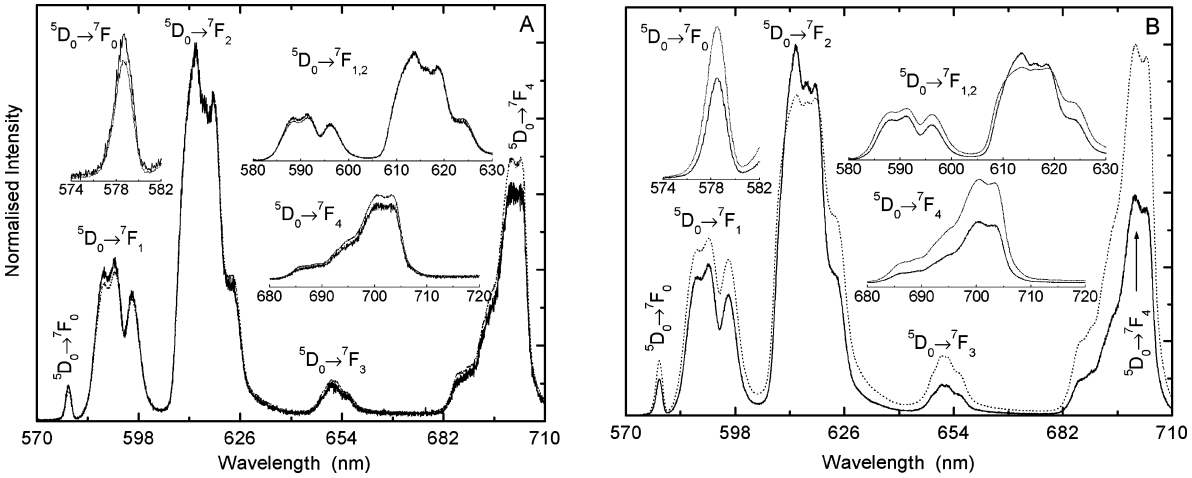

Figure 5. Low-temperature (14 K) emission spectra of the (A) Eu and (B) Eu−Gd apatite under different excitation wavelengths: 248 nm (solid line) and 393 nm (dotted line).

dimensional channel running along the *c* axis[31−33] (oxygen around 6h position) which results in a distortion of the local 6h site symmetry.

We also try to assign the 4f and 6h Eu^{3+} local coordination sites with the emission and excitation features discussed above. From the analyses of the luminescence data it was possible to identify that one Eu^{3+} local environment is preferentially excited though a LMCT band with the $^5D_0 \rightarrow {}^7F_2$ transition being the more intense one, and the other Eu^{3+} local environment, essentially excited via direct excitation into the intra $4f^6$ levels, presents an increase in the $^5D_0 \rightarrow {}^7F_{0,1,3,4}$ transitions with respect to the $^5D_0 \rightarrow {}^7F_2$ one. The relative intensity increase of the $^5D_0 \rightarrow {}^7F_{0,1,3,4}$ transitions, in particular, of the $^5D_0 \rightarrow {}^7F_4$ one, as mentioned above, was recently attributed to the distortion of the Eu^{3+} local symmetry group toward a pure inversion center. According to the structural data, the Eu^{3+} local symmetry group, which is closer to an inversion center, is the one corresponding to the 6h position. Moreover, the unit cell parameters suggest that the 4f position is more populated with Gd^{3+} ions than with Eu^{3+} ions in the Eu−Gd apatite (see Rietveld Refinement section). Thus, in the Eu−Gd apatite a higher relative contribution of the Eu^{3+} ions in the 6h position than in the 4f site is expected. This is in good agreement with the higher relative contribution of the $^5D_0 \rightarrow {}^7F_4$ transition in the emission spectra of the Eu−Gd apatite, when compared with that of the Eu apatite. Further arguments supporting the above assignment are based on the work of Blasse and Brill on luminescent apatites.[15] These authors reported that the 4f site lacks a pronounced linear crystal field term, inducing very weak $^5D_0 \rightarrow {}^7F_{0,4}$ transitions, the $^5D_0 \rightarrow {}^7F_2$ one being more intense.[15]

The $^5D_0$ lifetimes were monitored at room temperature within the $^5D_0 \rightarrow {}^7F_{2,4}$ transition lines at 614 and 701 nm, respectively. The decay curves were well-reproduced by single-exponential functions (not shown), revealing for the Eu apatite and the Eu−Gd apatite $^5D_0$ lifetime values of $0.049/0.052 \pm 0.001$ and $0.227/0.2731 \pm 0.002$ for monitoring wavelengths within the $^5D_0 \rightarrow {}^7F_2/{}^7F_4$ transition lines, respectively. The dependence of the $^5D_0$ lifetime on the monitoring wavelength is in good agreement with the presence of two Eu^{3+} distinct local environments. The dilution with Gd^{3+} ions contributes to the enhancement of the lifetime value, strongly suggesting that concentration quenching may occur in the Eu apatite.

3.4. Absolute Emission Quantum Yields. The absolute emission quantum yield was estimated for the Eu and the Eu−Gd apatites, under the excitation wavelength that maximizes the emission intensity (395 nm) and within the LMCT states (255 nm). The estimated quantum yield values for the Eu apatite are 15.8 and 9.3% and for the Eu−Gd apatite they are 21.4 and 14.4% at 395 and 255 nm excitation wavelength, respectively.

There are few reports dealing with the estimation of the emission quantum yields in silicate materials activated by Eu^{3+} ions.[16] The values known for Eu^{3+} silicate materials with hexagonal structure ranges from 6 to 15% for the host lattices $LiLaSiO_4$ and $LiGdSiO_4$, respectively, under excitation into the respective LMCT charge-transfer band.[16] The variations in the quantum yield values were explained in terms of the LMCT energy peak position, in such a way that the emission quantum is higher if the LMCT states move to shorter wavelengths.[16] The LMCT band of the Eu^{3+}-activated $LiLaSiO_4$ and $LiGdSiO_4$ materials peaks at ca. 280 and 265 nm, respectively. These LMCT energy levels are at higher wavelengths than those observed for the Eu^{3+} apatite silicates reported here (248 nm, Figure 4); thus, we should expect higher quantum yield values for the Eu and the Eu−Gd apatites. However, the quantum yields reported in this work are only slightly higher than those of the Eu^{3+}-activated $LiLaSiO_4$ and $LiGdSiO_4$ materials. It should be noted that the Eu^{3+} concentration in the $LiLaSiO_4$ and $LiGdSiO_4$ host is 2% and in the case of the Eu apatite and the Eu−Gd apatite the amount of Eu^{3+} is 100 and 40%, respectively. The presence of such high amounts of Eu^{3+} may contribute to the presence of extra nonradiative channels such as concentration quenching effects that may not be

(31) Tolchard, J.; Sansom, J. H.; Islam, M. S.; Slater, P. R. *Dalton Trans.* **2005**, 1273.
(32) Slater, P. R.; Sansom, J. E. H.; Tolchard, J. R. *Chem. Rec.* **2004**, *4*, 373.
(33) Leon-Reina, L.; Losilla, E. R.; Martinez-Lara, M.; Bruque, S.; Aranda, M. A. G. *J. Mater. Chem.* **2004**, *14*, 1142.

present at lower Eu^{3+} amounts, and thus contribute to lower emission quantum yields.

Comparing the quantum yield values of the Eu apatite and the Eu−Gd apatite, an increase (ca. 30%) is observed for the Gd diluted sample, which is further evidence supporting the fact that the incorporation of Gd^{3+} ions in the Eu apatite contributes to decreasing quenching effects.

4. Conclusion

For the first time lanthanide silicates $Eu_{8.18}Na_{1.08}(SiO_4)_6(OH)_{1.62-2y}O_y$ and $Eu_{3.96}Gd_{3.96}Na_{1.2}(SiO_4)_6(OH)_{1.86-2y}O_y$ with the apatite-type structure were synthesized at mild hydrothermal conditions. Both silicates were analyzed by Rietveld refinement, suggesting a preferential substitution of Ln^{3+} ions by Na^+ ions in the 4f position for both materials and more pronounced for the Eu one. This distribution of the Na^+ ions causes a decrease of local positive charge around OH^- ions, which is expressed in a shift of the 4e position. The inclusion of Gd^{3+} ions dilutes the Eu^{3+} content and alters the distribution of Ln^{3+} ions between 4f and 6h sites, which impacts their local symmetry and optical properties. The emission features, in particular the abnormal increase in the relative intensity of the Eu^{3+} intra-$4f^6$ $^5D_0 \rightarrow {}^7F_4$ transition, point out the presence of interstitial oxygen or incommensurate ordering of the oxygen around the 6h position that results in distortion of the local symmetry. The $^5D_0$ level of Eu^{3+} is populated via a LMCT band involving $O^{2-} \rightarrow Eu^{3+}$ ligand-to-metal charge transfer (LMCT) states and through direct intra-$4f^6$ excitation. The absolute emission quantum yield depends on the selected excitation wavelength, ranging from 9.3 to 14.4%, under excitation through LMCT states and from 15.8 to 21.4% via direct excitation into the intra-$4f^6$ levels on the Eu and the Eu−Gd apatites, respectively. The quantum yield and the $^5D_0$ lifetime values also depend on the amount of Eu^{3+}, being smaller for the Eu apatite, suggesting the presence of concentration quenching effects. Such Eu^{3+} concentration quenching effects were reduced by the incorporation of Gd^{3+} cations.

Acknowledgment. This work was supported by Fundação para a Ciência e Tecnologia (FCT), Programa Operacional "Ciência, Tecnologia, Inovação" (POCTI) and NoE FAME. S.F. also thanks FCT (SFRH/BPD/23771/2005) for the grant. O. L. Malta and L. D. Carlos are gratefully acknowledged for fruitful discussions concerning the photoluminescence data.

CM0617384